Atomic structure of chlorine containing calcium silicate glasses by neutron diffraction and ^{29}Si solid state NMR.

Louis F Chungong[1], Laura A Swansbury[2], Gavin Mountjoy[2], Alex C Hannon[3], Adam F Lee[1], Richard A Martin*[1]

[1]Aston Institute of Materials Research, School of Engineering & Applied Science and Aston Research Centre for Healthy Ageing, Aston University, Birmingham B4 7ET, UK

[2]School of Physical Sciences, University of Kent, Canterbury, CT2 7NH, UK

[3]ISIS Facility, Science and Technology Facilities Council. Rutherford Appleton Laboratory, Harwell Science and Innovation Campus, Didcot, Oxfordshire, OX11 0QX, UK.

*R.A.Martin@Aston.ac.uk

Abstract

Bioactive glasses are of great importance for medical and dental applications. In order to understand, model and predict the behaviour of these materials, and ultimately improve their design, it is important to understand the structure of these glasses. Ion dissolution is known to be the crucial first step in bioactivity and is strongly dependent upon the atomic scale structure and network connectivity. Whilst significant progress has been made understanding the structure of oxide based glasses, relatively little is known about the structure of bioactive glasses containing halides. Recently a series of novel chloride based bioactive glasses has been developed. Chlorapatite converts to hydroxyapatite in water and these glasses are therefore of interest for novel toothpastes. This study reports the first detailed structural investigation of these bioactive chloride glasses using neutron diffraction and solid state NMR. Chlorine was found to bond to calcium within the glass, and no evidence of Si-Cl bonding was detected. Furthermore, the absence of a chemical shift in the ^{29}Si NMR upon the addition of $CaCl_2$ helped confirm the absence of detectable amounts Si-Cl bonding. Given that chlorine does not disrupt the Si-O-Si network, widely used network connectivity models are therefore still valid in oxychloride glasses.

Introduction

Since the invention of bioglass by Larry Hench in 1969, bioactive glasses have been used for a range of medical and dental applications [1-3]. These glasses have the ability to chemically bond to bone and stimulate new bone growth [4, 5]. The reaction mechanisms are reasonably well understood for archetypal bioactive glasses. Controlled dissolution of the glass is the critical first step in the bioactivity of these materials. Traditional bioactive glasses consist of sodium calcium silicate glasses with the addition of small quantities of P_2O_5. Calcium ions are released from the silicate host and combine with phosphorous ions (either from the glass or from body fluid) to form an amorphous calcium phosphate layer which then crystallises into hydroxyapatite [6]. Sodium oxide is only incorporated into the glass to improve glass forming properties (lowering the melt temperature) and for aiding the dissolution of the glass. Oxygen atoms have a large affinity for bonding with silicon atoms, therefore the addition of oxygen atoms in the form of sodium and calcium oxide fragments the silicate network. The atomic-scale structure, its effect on the network connectivity, and the effects of these factors on the chemical durability and bioactivity has been widely studied and is reasonably well understood for sodium calcium phosphosilicates [7-9]. However other systems are less well studied.

Recently, Hill and co-workers have developed novel sodium free bioactive glasses containing halides for dental applications [10, 11]. Fluoride containing glasses have potential benefits for dental applications; for example the presence of CaF_2 favours the formation of fluorapatite which is more resistant to acid erosion. Consequently, fluoride doped bioactive glasses are already incorporated into toothpastes. However, high fluoride concentrations in bioactive glasses result in the formation of CaF_2 upon quenching [10]. Furthermore given that excess fluoride can potentially lead to fluorosis, the use of fluoride is highly regulated in toothpastes with an upper limit of 1500ppm in Europe [12].

Chen *et al.* have developed a series of novel $CaCl_2$ containing glasses as an alternative to the fluorides [10]. Replacing calcium fluoride with calcium chloride avoids the problems of excess CaF_2 in the glass and avoids regulatory restrictions since chlorides are naturally present in the human

body. Chlorapatite readily converts into hydroxyapatite on immersion in water making chloride containing bioactive glasses particularly attractive for incorporating into toothpaste.

In order to be able to model and predict the behaviour of these glasses and ultimately improve their design it is important to understand the local structure of these novel glasses and in particular the role chlorine adopts in these glasses. The structure will strongly influence the release kinetics and dissolution profile however it is not possible to predict *a prior* the structure of these glasses.

There have been reports that F can bond directly to Si in calcium fluorosilicates; e.g. Iwamoto *et al*. [13] found that F ions bond to Si at low CaF_2 concentrations (< 7 mol %), and Tsunawaki reported that Si-O bonds were still broken for concentrations up to 15-20 mol% CaF_2 [14]. However the large size difference between Cl and F ions means they could adopt significantly different structural roles. Again there are conflicting reports of the role Cl may adopt within these glasses; for example Rabinovich *et al.* [15] hypothesised that Cl^- can replace bridging oxygen atoms due to their polarizability whilst Sandland *et al.* reported chloride ions were primarily coordinated to Ca^{2+} in calcium silicate glasses [16].

We have therefore investigated a series of $CaCl_2$ containing glasses using a combination of neutron diffraction and solid state NMR. Glasses of composition $(SiO_2)_{50-x/2}(CaO)_{50-x/2}(CaCl_2)_x$, where x varies between 3.3 and 27.4 were designed to keep a constant Si:O ratio to enhance sensitivity to any structural differences in the silicate network caused by the addition of $CaCl_2$.

Methods

Glass preparation

Melt quenched glass samples were prepared using SiO_2 (Alfa Aesa, 99.5%), $CaCl_2.2H_2O$ (Sigma Aldrich ≥ 99.999%) and $CaCO_3$ (Alfa Aesar, 99.95-100.05%) precursors. After weighing the precursors in the appropriate molar concentrations the chemicals were thoroughly mixed and placed into a 90%Pt-10%Rh crucible. The crucible and precursors were then heated, under an inert flowing argon atmosphere, from room temperature to a final temperature of between 1320°C and 1530°C with a heating rate of 10°C/minute. After homogenising for 1 hour at temperature, the

liquid melts were rapidly splat quenched between two carbon graphite blocks to form glasses. The mass of the resultant glass was measured and compared with expected values, based on the mass of the starting precursors, to ensure no unexpected losses occur during the heating process. Excess argon prevented oxidation during the heating process. To avoid potential absorption of moisture from air, the glasses were stored in a desiccator. Glass densities were measured using a He pycnometer (Quantachrome Multipycnometer). The nominal glass compositions, melt temperatures and glass densities are given in Table 1.

Table 1. Nominal compositions, melt temperatures and densities of the glass series.

Glass code	Nominal glass composition (mol %)			Melting temp. (°C)	Density (g/cm^3)
	SiO_2	CaO	$CaCl_2$		
GCl 3.3	0.484	0.484	0.033	1530	2.99
GCl 6.6	0.467	0.467	0.066	1480	2.96
GCl 9.3	0.453	0.453	0.093	1490	2.91
GCl 11.9	0.441	0.441	0.119	1480	2.94
GCl 16.1	0.419	0.419	0.161	1470	2.82
GCl 27.4	0.363	0.363	0.274	1445	2.75

Neutron diffraction

Neutron diffraction spectra were collected using the GEM diffractometer at the ISIS spallation neutron source at the Rutherford Appleton Laboratory, UK [17]. The coarsely ground samples were held at ambient temperature in a cylindrical vanadium container of 8.3 mm internal diameter and 0.025 mm wall thickness. Interference patterns were collected for each of the samples, an empty vanadium container, an 8 mm diameter vanadium niobium null alloy (0.941V: 0.059Nb) and the empty GEM instrument in order to perform the appropriate corrections. Data corrections including background scattering, inelastic, multiple and self-scattering were performed using GUDRUN [18].

Following these corrections, the resultant coherent scattering intensity, $i(Q)$, is defined by

$$i(Q) = \sum_i \sum_j c_i c_j b_i b_j \left[p_{ij}(Q) - 1\right] \quad (1)$$

where c_i, c_j, b_i and b_j represent the atomic concentration and coherent scattering length of the chemical species *i* and *j* respectively, and $p_{ij}(Q)$ is the pair correlation function. Fourier transforming $i(Q)$ generates the total correlation function, $T(r)$, given by

$$T(r) = T^0(r) + \frac{2}{\pi}\int_0^\infty Qi(Q)M(Q)\sin(Qr)\,dQ \quad (2)$$

where $M(Q)$ is a Lorch window function that takes into account the finite maximum experimentally attainable value of Q. $T^0(r)$ is the average density term, given by:

$$T^0(r) = 4\pi r\rho^0(\textstyle\sum_i c_i b_i)^2 \quad (3)$$

where r is the distance from an arbitrary atom at the origin and ρ^0 is the atomic number density.

Structural information can be obtained by modelling the real-space correlation functions. Pair functions are generated in Q-space and Fourier transformed to allow comparison with the experimental data in real-space. The pair functions are given by:

$$p_{ij}(Q)_{ij} = \frac{N_{ij}w_{ij}}{c_j}\,\frac{\sin Q\,r_{ij}}{Q\,r_{ij}}\exp\left[\frac{-Q^2\sigma_{ij}^2}{2}\right] \quad (4)$$

where N_{ij}, r_{ij} and σ_{ij} represent the coordination number, atomic separation and disorder parameters respectively. The weighting factor w_{ij} is given by:

$$w_{ij} = 2c_i c_j b_i b_j \quad \text{if } i \neq j \quad (5)$$

$$w_{ij} = c_i^2 b_i^2 \quad \text{if } i = j \quad (6)$$

Atomic bond distances, coordination numbers and disorder were fitted using NXFit [19].

^{29}Si NMR

Solid state NMR spectra were obtained at the EPSRC UK National Solid-state NMR service at Durham on a 4.0 MM pencil Varian VNMRS 400 MHz spectrometer. The observed ^{29}Si spectra were acquired with a frequency of 79.438 MHz, spectral width of 40322.6 Hz, acquisition time of 12.7 ms, and repetitions in the range 56-800 with a recycling time of 120 s at ambient temperature. Direct excitation had a pulse duration of 4.6 µs with a two pulse phase modulated decoupling [20] spin rate of 6000 Hz with reference to tetramethylsilane (0 ppm) [21].

Results and discussions

The series of calcium silicate glasses containing $CaCl_2$ were successfully prepared by splat quenching between two carbon graphite blocks. In contrast to samples quenched into open graphite moulds, which showed visible signs of crystallisation and were therefore discarded, glasses quenched between two graphite plates were visibly clear and homogenous and showed no sign of crystallisation. Splat quenching avoided the need to quench into water which is highly undesirable given that these glasses are hydroscopic and water soluble. Furthermore neutron scattering is very sensitive to hydrogen which gives rise to large inelastic scattering and can be difficult to accurately correct for.

Density as a function $CaCl_2$ content is given in Figure 1. As shown there is a systematic decrease in density of the series as the $CaCl_2$ content increased. In contrast the molar volume increases with increasing $CaCl_2$ concentrations. Similar trends of reduced density and increased molar volume as a function of $CaCl_2$ were reported by Chen [22].

Neutron diffraction.

Neutron interference functions, *i*(Q), for the $(SiO_2)_{50-x/2}(CaO)_{50-x/2}(CaCl_2)_x$ series are shown in Figure 2. Although the reciprocal space data extends to 50 $Å^{-1}$ only $0 < Å^{-1} < 30$ is shown for clarity. Figure 3 shows the corresponding real space correlation function, *T*(r), obtained by Fourier transforming the reciprocal space *i*(Q) functions given in Figure 2 over the full range of 0 to 50 $Å^{-1}$. The first peak in real space at ~ 1.6 Å corresponds to the well-defined Si-O tetrahedra. Given the size of the atoms, it is anticipated that a Si-Cl peak would occur in the region ~2.0 Å [23]. The absence of any notable features in this region suggests there is minimal direct bonding between silicon and chlorine at this detection level. As a result it is assumed that only interlinking SiO_4 tetrahedra form the network structure of the glasses.

The second principal feature in real space is more complex and contains overlapping O-(Si)-O and Ca-O correlations, of which the Ca-O can be further refined into bridging ($Ca\text{-}O_B$) and non-bridging (CaO_{NB}) correlations. In addition, Ca-Cl peaks would be expected to appear in this region. The

position of the O-(Si)-O correlation is reasonably well defined by the geometry of the SiO_4 tetrahedra given by $\sqrt{8/3}\ r_{Si-O}$, being ~ 2.65 Å. The O-(Si)-O coordination number can also be modelled using connectivity models and confirmed using ^{29}Si NMR. For a silicate glass the network connectivity (NC) is given by

$$NC = 4 - 2Z, \quad (7)$$

where Z, the number of excess oxygen per SiO_2, and is given by

$$Z = \frac{c_O}{c_{Si}} - 2 \quad (8)$$

where c_O and c_{Si} represent the concentration of oxygen and silicon respectively.

Solid state NMR

Figure 4 shows the solid state ^{29}Si NMR. Spectra are similar for all of the chloride containing glasses, and have a broad peak at ~ -81ppm which is assigned to a Q^2 connectivity. The Q^2 species full linewidth at half-height of ~13 ppm causes significant spectral overlap with the corresponding Q^1 and Q^3 chemical shift regions and precludes their independent observation if they are present at low concentrations. Importantly, only the average Q^n species is required to calculate the O–(Si)–O coordination number given in the model. In previous ^{29}Si NMR studies on bioactive glasses linewidths of ~ 12ppm corresponded to less than 3% Q^1 or Q^3. In pure SiO_2 the network connectivity is 4 as shown in Figure 5 (left) and Figure 6. Each of the oxygen atoms are bridging (i.e. bonded to two silicon atoms). The addition of further oxygen atoms in the form of CaO depolymerises the Si-O-Si network as shown in Figure 5 (right). A single additional oxygen atom per two Si tetrahedra reduces the network connectivity from Q^n to Q^{n-1}. As illustrated a single CaO for two silica units reduced the connectivity from Q^4 to Q^3. In the present system, given in Table 1, the glasses have a fixed Si:O ratio of 1:3 (due to a SiO_2:CaO ratio of 1:1), i.e. there is one excess oxygen per silica, or two excess oxygen atoms per two silica units. It is therefore anticipated that the glasses would adopt a Q^2 structure (Figure 6).

The absence of any significant difference in chemical shifts between samples (Fig. 4), combined with the absence of any notable Si-Cl peak in the region ~2 Å (Fig. 3) strongly suggests that chlorine atoms do not bond directly to silicon atoms. In addition this shows that $CaCl_2$ is not oxidised into CaO during the manufacturing process, as any oxidation would have changed the Si:O ratio (as shown in Figure 5) and therefore change the ^{29}Si chemical shift. Coupled with knowledge of the Q speciation allows the average O–(Si)–O coordination number to be calculated. A bridging O atom has six next nearest neighbour O atoms whilst a non-bridging O has only three next nearest neighbour O atoms as shown in Figure 5. It can therefore be calculated that the average O–(Si)–O coordination number for a metasilicate (Q^2) glass is 4.0. The complex overlapping region 2.2 < r (Å) < 2.8 has therefore been simplified by applying the network connectivity model and verified using ^{29}Si NMR.

Fits for GCl 6.6 and GCl 16.1, representative of low and high $CaCl_2$ concentrations, are shown in Figure 7 and the corresponding fitting parameters are given in Table 2. Table 2 shows the Si-O peak at ~ 1.63 Å is constant for all of samples independent of the addition of $CaCl_2$. As the $CaCl_2$ concentration increases, the disordering in SiO_4 tetrahedra remains almost constant. The Si-O coordination number remains ~4.0(1) for all the samples, showing that each Si is surrounded by a tetrahedra of oxygen atoms. If Cl atoms had replaced O atoms within the tetrahedra a subsequent reduction in the Si-O coordination number would have been anticipated in order to accommodate the Si-Cl bonds. In addition there are no obvious features at ~ 2.0 Å where potential Si-Cl correlations would have been expected to occur. The Si-O distance agrees with mean Si-O distance of 1.63 Å in crystalline calcium chlorosilicate $Ca_2SiO_2Cl_2$ and wollastonite $Ca_3Si_3O_9$ [24, 25]. Whilst Rabinovich *et al.* [15] hypothesised that Cl^- atoms are capable of replacing all the O atoms within the SiO_4 network at higher synthesis temperatures based on their polarizability no evidence of this is found here. Furthermore our results are in agreement with the ^{35}Cl MAS NMR results of Sandland *et al.*[16] who reported chloride ions were primarily coordinated to Ca^{2+} in calcium silicate glasses with no significant Si-Cl bonds being detected. The present results are also in agreement with the recent molecular dynamic simulations of $CaO\text{-}SiO_2\text{-}CaCl_2$ glass by Swansbury *et al.* who reported an absence of direct Si-Cl bonding [26].

Table 2. Neutron diffraction structural parameters obtained by fitting *T*(r).

Glass	SiO			CaO_{NB}			O-(Si)-O			CaO_B			CaCl		
	r(Å)	N	σ(Å)	r(Å)	N	σ(Å)	r(Å)	N	σ(Å)	r(Å)	N	σ(Å)	r(Å)	N	σ(Å)
GCl 3.3	1.63	4.0	0.06	2.37	5.2	0.13	2.65	4.1	0.10	2.76	1.3	0.08	2.79	0.3	0.10
GCl 6.6	1.63	4.0	0.06	2.37	5.0	0.13	2.65	4.0	0.10	2.75	1.4	0.10	2.78	0.6	0.12
GCl 9.3	1.63	4.1	0.06	2.38	4.8	0.14	2.66	4.0	0.10	2.74	1.2	0.11	2.78	0.7	0.10
GCl11.9	1.63	4.0	0.05	2.37	4.8	0.14	2.66	4.1	0.10	2.76	1.2	0.12	2.77	0.9	0.10
GCl16.1	1.63	4.1	0.05	2.37	4.5	0.13	2.64	4.0	0.10	2.75	1.1	0.13	2.78	1.2	0.11
GCl27.4	1.63	4.1	0.06	2.36	3.5	0.13	2.65	3.9	0.10	2.75	1.0	0.14	2.79	2.1	0.12

The Ca-O environment is split into non-bridging and bridging correlations at ~ 2.37(2) and 2.75(1) Å respectively with O_{NB} coordination numbers decreasing from 5.2(2) to 3.5(2) and O_B decreasing from 1.4 to 1.0(2) upon the addition of $CaCl_2$ as shown in Figure 8. Values for the lowest content Cl glass, GCl3.3, are in reasonable agreement with previous reports for a range of calcium silicate bioactive glasses [27-29] where values O_{NB} and O_B coordination numbers of 5.3 and 1.3 were reported. Ca-Cl correlations were observed ~ 2.78(1) Å in broad agreement with distances reported for crystalline $Ca_2SiO_3Cl_2$ (equivalent to x = 0.33 in our system) where values of 2.76, 2.77, 2.81 and 2.82 Å were observed[24].

As expected, the average number of Cl atoms surrounding Ca significantly increases (from 0.3 to 2.1) as the concentration of $CaCl_2$ increases, while the average number of O atoms decreases in anti-correlation (Figure 8). Despite these structural changes, the average total number of atoms surrounding a calcium atom remains constant at ~6.8(1) which is in good agreement with the calcium polyhedra reported for crystalline $Ca_2SiO_3Cl_2$.

The diffraction data provides an average of the structure and gives mixed Ca-O/Cl polyhedra as anticipated. For example, in crystalline $Ca_2SiO_3Cl_2$ mixed calcium polyhedra were observed where each calcium atom was bonded to 4 oxygen atoms and 3 chlorine atoms thereby giving a total Ca coordination number of 7 [24]. However whilst there is no evidence of phase separation from this study it is worth noting that Swansbury *et al*. have recently reported that phase separation can occur for $CaCl_2$ concentrations above 16.1. Small angle scattering would be needed to unambiguously determine any phase separation. However it is interesting to note that when the Ca-O/Cl coordination numbers are scaled by the relative concentrations of O and Cl (to mimic phase separation) then the Ca-O_{NB} and Ca-O_B coordination numbers are constant for all the glass samples at 5.5(1) and 1.5(1) respectively and Ca-Cl coordination number is constant at 6.2(1). This scaling enables a direct comparison with previous structural data on the Ca-O_{NB} and Ca-O_B coordination numbers reported for halide free bioactive glass systems [8, 9]. As expected the Ca-O_{NB} and Ca-O_B coordination numbers results after scaling are reasonably close to those of GCl3.3 the lowest content $CaCl_2$ glass.

As anticipated the Ca-Cl correlations are best resolved for glasses containing larger concentrations of $CaCl_2$. It is clear that the accuracy of the Ca-Cl peak clearly influences the overall fit as shown in supplementary Figure 1 and that the Ca-Cl fit is highly robust for the higher $CaCl_2$ concentration glasses.

Bond valence parameters can also be used to verify the local environment of calcium [30]. Using the bond valence method the valence of a cation can be calculated using

$$V_i = \sum_j v_{ij} = \sum_j exp\left[\frac{R_{ij} - r_{ij}}{B}\right] \quad (9)$$

where v_{ij} is the bond valence between atom *i* and j, *B* is an empirical constant (0.37) and R_{ij} is the bond valence parameter for the atom pair *i*,*j*. R_{ij} values of R_{CaO} =1.967 Å and R_{CaCl} = 2.37 Å are given by Bresse and O'Keefee [31]. r_{ij} values for $r_{Ca\text{-}ONB}$, $r_{Ca\text{-}OB}$ and $r_{Ca\text{-}Cl}$ determined from the neutron diffraction (Table 2) allow the Ca valence to be calculated. Values of ~ 2.0(1) were calculated for all glass compositions further verifying the reliability of the Ca-O and Ca-Cl bond distances and coordination numbers obtained from neutron diffraction fitting.

Conclusions.

Si-O coordination numbers around 4.0(1) were recorded for samples. No structural features were observed in $T(r)$ at ~ 2.0 Å as would be expected for Si-Cl distances. We therefore conclude that Cl does not bond directly to Si and does not influence the network connectivity. Furthermore the chemical shift of ^{29}Si NMR remains constant ~ -81ppm, confirming that SiO_4 tetrahedral are unaffected by Cl addition, and that the Si-O-Si network connectivity is maintained independent of the addition of $CaCl_2$ into the glass. For the present materials, a meta-silicate Q^2 network is present. The addition of $CaCl_2$ does not impact the connectivity, and would therefore not be expected to impact upon dissolution of the silicate network. However, as the concentration of $CaCl_2$ increases the number of Ca-O bonds decreases as calcium coordinates to more Cl, and it is therefore anticipated that calcium will dissolve more rapidly from such glasses.

Acknowledgments

The authors would like to thank STFC for the provision of beam-time at the ISIS pulse neutron source [ref 1520055] and the Solid State NMR service, University of Durham, for solid state NMR experiments. The authors would also like to thank R G Hill and N Karpukhina for helpful scientific discussions.

References

1. Hench, L.L., *Chronology of Bioactive Glass Development and Clinical Applications.* New Journal of Glass and Ceramics, 2013. **Vol.03No.02**: p. 7.
2. Hench, L.L., *The story of Bioglass (R).* Journal of Materials Science-Materials in Medicine, 2006. **17**(11): p. 967-978.
3. Hench, L.L., et al., *Glass and Medicine.* International Journal of Applied Glass Science, 2010. **1**(1): p. 104-117.
4. Hench, L.L., Splinter, R. J., Allen, W. C. and Greenlee, T. K., *Bonding mechanisms at the interface of ceramic prosthetic materials.* Journal of Biomedical Materials Research Symposium, 1971. **5**: p. 25.
5. Clark, A.E., L.L. Hench, and H.A. Paschall, *Influence of Surface Chemistry on Implant Interface Histology - Theoretical Basis for Implant Materials Selection.* Journal of Biomedical Materials Research, 1976. **10**(2): p. 161-174.

6. Martin, R.A., et al., *A study of the formation of amorphous calcium phosphate and hydroxyapatite on melt quenched Bioglass(A (R)) using surface sensitive shallow angle X-ray diffraction.* Journal of Materials Science-Materials in Medicine, 2009. **20**(4): p. 883-888.
7. Hill, R., *An alternative view of the degradation of bioglass.* Journal of Materials Science Letters, 1996. **15**(13): p. 1122-1125.
8. Martin, R.A., et al., *An examination of the calcium and strontium site distribution in bioactive glasses through isomorphic neutron diffraction, X-ray diffraction, EXAFS and multinuclear solid state NMR.* Journal of Materials Chemistry, 2012. **22**(41): p. 22212-22223.
9. Martin, R.A., et al., *A structural investigation of the alkali metal site distribution within bioactive glass using neutron diffraction and multinuclear solid state NMR.* Physical Chemistry Chemical Physics, 2012. **14**(35): p. 12105-12113.
10. Chen, X., et al., *Novel Highly Degradable Chloride Containing Bioactive Glasses.* Biomedical glasses, 2015. **1**(1).
11. Chen, X., R. Hill, and N. Karpukhina, *Chlorapatite Glass-Ceramics.* International Journal of Applied Glass Science, 2014. **5**(3): p. 207-216.
12. Jabbarifar, S.E., et al., *Effect of fluoridated dentifrices on surface microhardness of the enamel of deciduous teeth.* Dental research journal, 2011. **8**(3).
13. Iwamoto, N. and Y. Makino, *A structural investigation of calcium fluorosilicate glasses.* Journal of Non-Crystalline Solids, 1981. **46**(1): p. 81-94.
14. Tsunawaki, Y., et al., *Analysis of CaO・SiO2 and CaO・SiO2・CaF2 glasses by Raman spectroscopy.* Journal of Non-Crystalline Solids, 1981. **44**(2-3): p. 369-378.
15. Rabinovich, E., *On the behavior of fluorine in silicate glasses.* Izv. Akad. Nauk SSSR, Neorg. Mater, 1967. **3**(5): p. 855-859.
16. Sandland, T.O., et al., *Structure of Cl-containing silicate and aluminosilicate glasses: A 35 Cl MAS-NMR study.* Geochimica et Cosmochimica Acta, 2004. **68**(24): p. 5059-5069.
17. Hannon, A.C., *Results on disordered materials from the GEneral Materials diffractometer, GEM, at ISIS.* Nuclear Instruments & Methods in Physics Research Section a-Accelerators Spectrometers Detectors and Associated Equipment, 2005. **551**(1): p. 88-107.
18. McLain, S., et al., *GUDRUN, a computer program developed for analysis of neutron diffraction data.* ISIS Facility, Rutherford Appleton Laboratory, Chilton, UK.
19. Pickup, D., R. Moss, and R. Newport, *NXFit: a program for simultaneously fitting X-ray and neutron diffraction pair-distribution functions to provide optimized structural parameters.* Journal of Applied Crystallography, 2014. **47**(5): p. 1790-1796.
20. Bennett, A.E., et al., *Heteronuclear decoupling in rotating solids.* The Journal of Chemical Physics, 1995. **103**(16): p. 6951-6958.
21. Harris, R.K., et al., *NMR nomenclature: nuclear spin properties and conventions for chemical shifts. IUPAC Recommendations 2001. International Union of Pure and Applied Chemistry. Physical Chemistry Division. Commission on Molecular Structure and Spectroscopy.* Magnetic Resonance in Chemistry, 2002. **40**(7): p. 489-505.
22. Chen, X., et al., *High chloride content calcium silicate glasses.* Physical Chemistry Chemical Physics, 2017. **19**(10): p. 7078-7085.
23. Masatoki, Y., *Electron Diffraction Investigation on the Molecular Structures of Some Organosilicon Compounds. I.* Bulletin of the Chemical Society of Japan, 1957. **30**(1): p. 100-106.
24. Golovastikov, N. and V. Kazak, *CRYSTAL-STRUCTURE OF CALCIUM CHLOROSILICATE CA2SIO3CL2.* Kristallografiya, 1977. **22**(5): p. 962-965.
25. Hesse, K.-F., *Refinement of the crystal structure of wollastonite-2M (parawollastonite).* Zeitschrift für Kristallographie-Crystalline Materials, 1984. **168**(1-4): p. 93-98.
26. Swansbury, L.A. and G. Mountjoy, *Modeling the Onset of Phase Separation in CaO-SiO2-CaCl2 Chlorine-Containing Silicate Glasses.* 2017.
27. FitzGerald, V., et al., *A neutron and X-ray diffraction study of bioglass with reverse Monte Carlo modelling.* Advanced Functional Materials, 2007. **17**(18): p. 3746-3753.
28. Smith, J.M., et al., *Structural characterisation of hypoxia-mimicking bioactive glasses.* Journal of Materials Chemistry B, 2013. **1**(9): p. 1296-1303.

29. Martin, R.A., et al., *Structural characterization of titanium-doped Bioglass using isotopic substitution neutron diffraction.* Physical Chemistry Chemical Physics, 2012. **14**(45): p. 15807-15815.
30. Brown, I.D. and D. Altermatt, *Bond-valence parameters obtained from a systematic analysis of the Inorganic Crystal Structure Database.* Acta Crystallographica Section B, 1985. **41**(4): p. 244-247.
31. Brese, N. and M. O'keeffe, *Bond-valence parameters for solids.* Acta Crystallographica Section B: Structural Science, 1991. **47**(2): p. 192-197.

Figure captions

Fig. 1**.** Density and molar volume as a function of $CaCl_2$ concentration.

Fig. 2. Reciprocal space functions i(Q) for the glasses. Q space extends to 50 $Å^{-1}$ only 0 < Q ($Å^{-1}$) < 30 is shown for clarity.

Fig. 3. Real space functions T(r). Data sets are offset for clarity.

Fig. 4. ^{29}Si NMR chemical shifts. Data sets are offset for clarity.

Fig. 5. A schematic of the structural changes in a silicate upon the addition of oxygen atoms in the form of CaO.

Fig. 6. Illustration of the Q species based on the number of bridging oxygen atoms (O-Si-O). As shown a bridging oxygen (O_B) has 6 next nearest neighbour oxygen atoms compared to just 3 for a non-bridging oxygen (O^-).

Fig. 7. The real space total diffraction patterns, $T(r)$ and the individually fitted pair correlation functions for GCl6.6 and GCl16.1.

Fig. 8. The average coordination number of bridging and non-bridging oxygen atoms and chlorine atoms surrounding a calcium atom.

Supplementary Figure 1. The real space total diffraction pattern and corresponding fit for GCl27.4. The CaCl peak has been omitted from the left hand side figure and it is clear that the model breaks down at ~ 2.5 Å. In contrast the right hand side figure includes the CaCl peak and as shown the fit is significantly better and the total fit and experimental data are in agreement to ~ 2.8 Å.

Figures

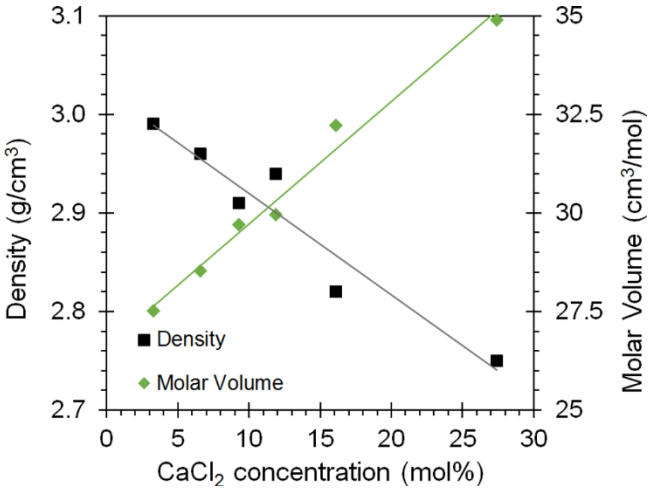
Density (g/cm3)
Molar Volume (cm3/mol)
CaCl2 concentration (mol%)
Density
Molar Volume

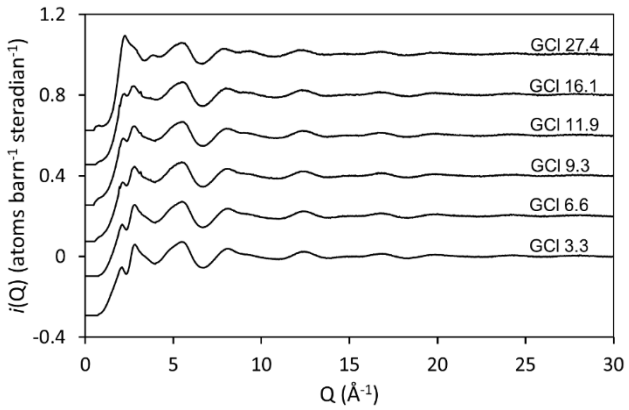
i(Q) (atoms barn-1 steradian-1)
Q (Å-1)
GCl 27.4
GCl 16.1
GCl 11.9
GCl 9.3
GCl 6.6
GCl 3.3

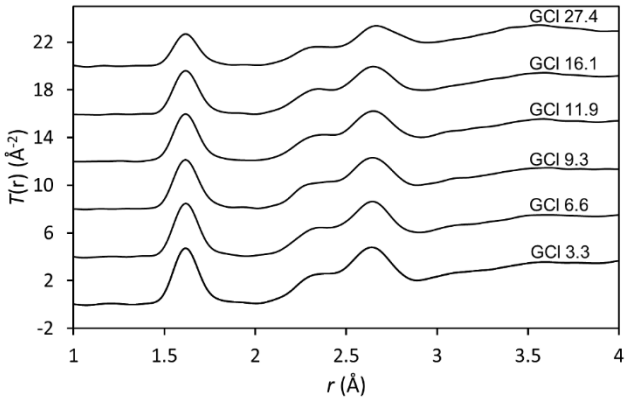
T(r) (Å-2)
r (Å)
GCl 27.4
GCl 16.1
GCl 11.9
GCl 9.3
GCl 6.6
GCl 3.3

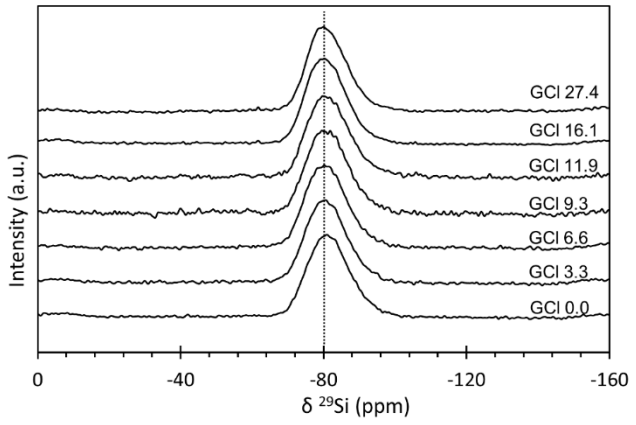
Intensity (a.u.)
δ 29Si (ppm)
GCl 27.4
GCl 16.1
GCl 11.9
GCl 9.3
GCl 6.6
GCl 3.3
GCl 0.0

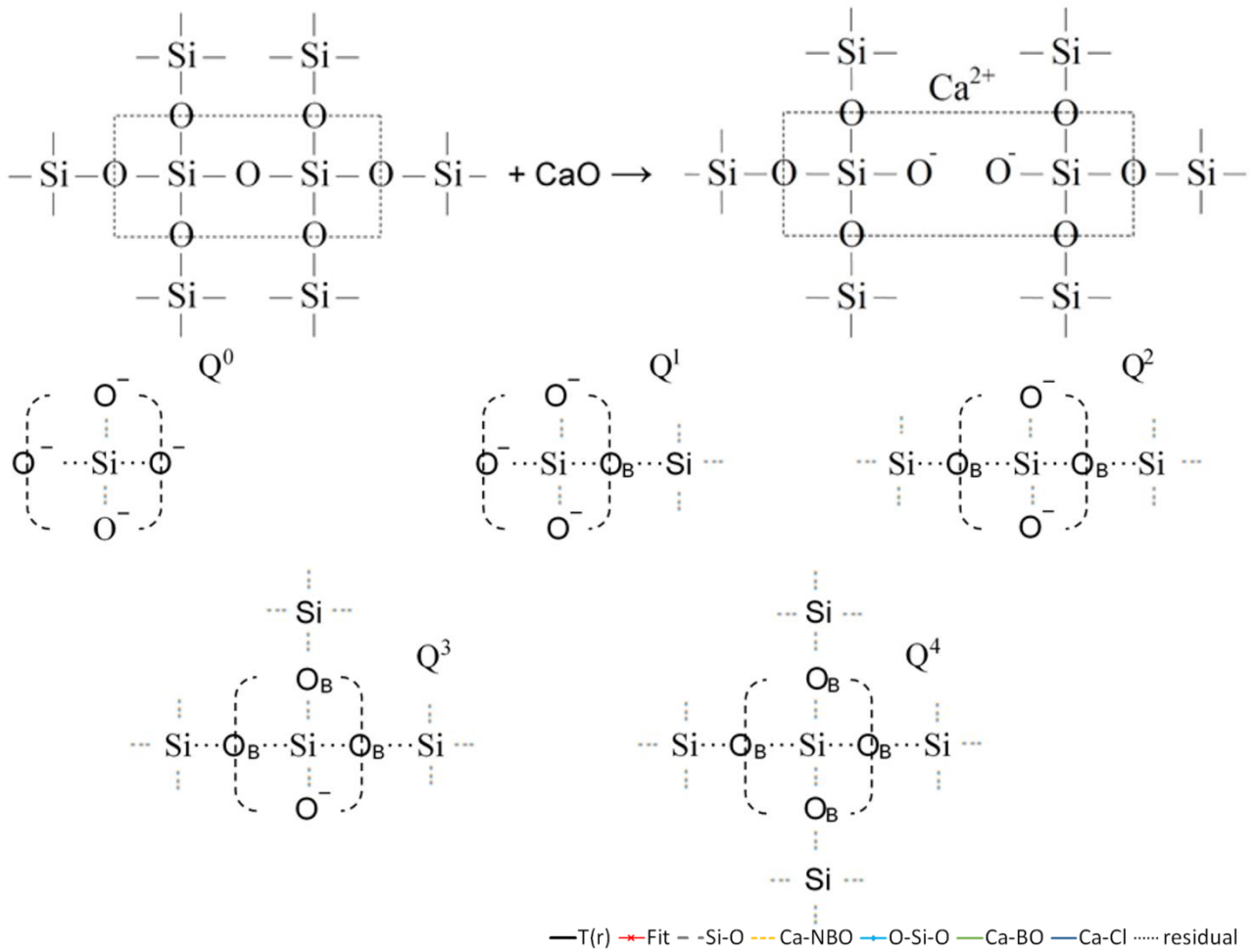
+ CaO
Ca2+
Q0
Q1
Q2
Q3
Q4

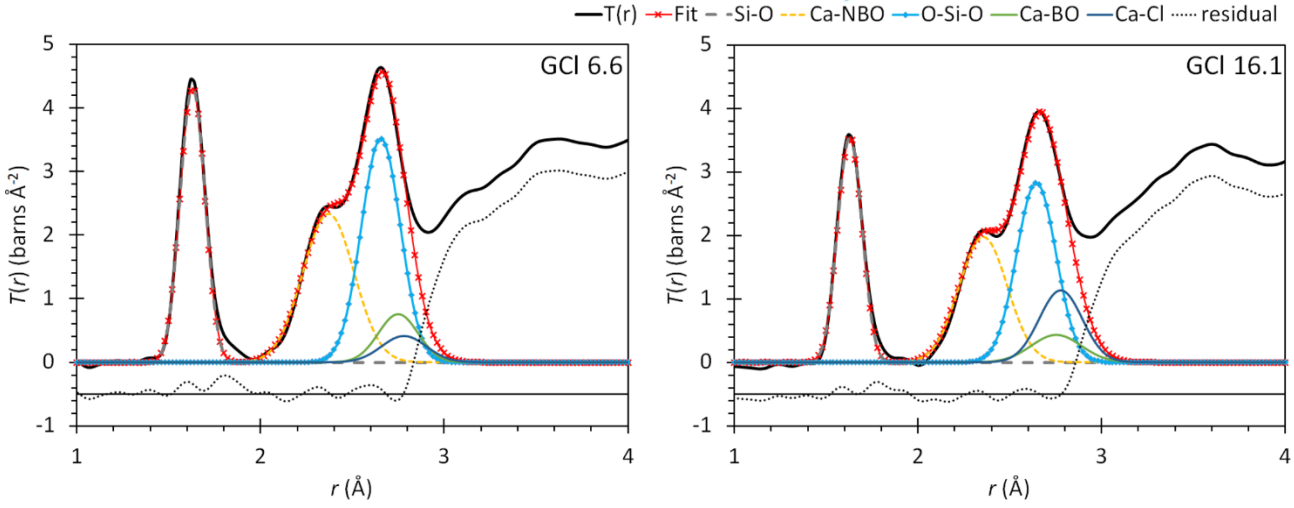
T(r)
Fit
Si-O
Ca-NBO
O-Si-O
Ca-BO
Ca-Cl
residual
GCl 6.6
GCl 16.1
T(r) (barns Å-2)
r (Å)

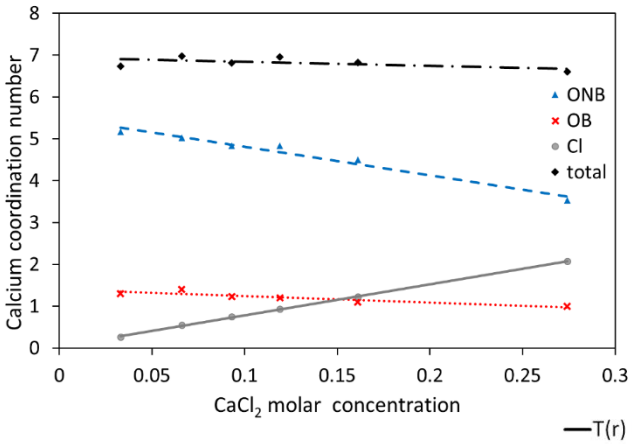
Calcium coordination number
CaCl2 molar concentration
ONB
OB
Cl
total

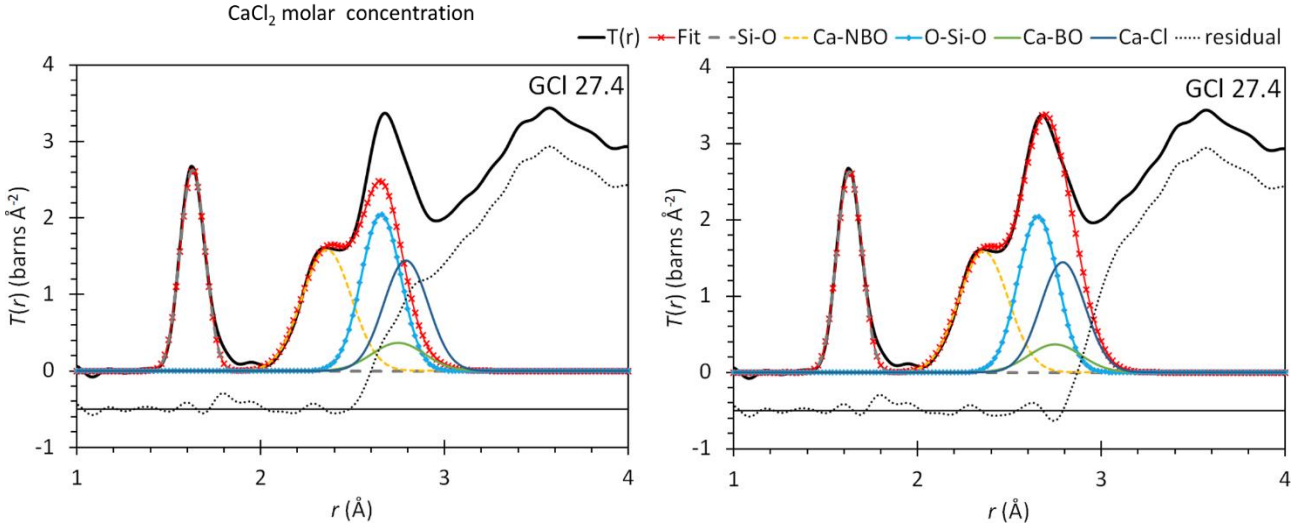
T(r)
Fit
Si-O
Ca-NBO
O-Si-O
Ca-BO
Ca-Cl
residual
GCl 27.4
T(r) (barns Å-2)
r (Å)
GCl 27.4
T(r) (barns Å-2)
r (Å)